20

Non-Isolated High-Gain DC-DC Converter Using Charge Pump and Coupling Inductor

Kuo-Ing Hwu and Yeu-Torng Yau
National Taipei University of Technology
Department of Electrical Engineering
Taiwan

1. Introduction

As generally acknowledged, the high-gain DC-DC converter is widely used in the sustainable energy system as the front-stage of the DC-AC converter. Therefore, it is indispensable for low voltage to be boosted to high voltage. In general, the boost converter or the buck-boost converter is widely used in such applications. However, it is not easy for such converters to achieve high voltage ratio. In theory, the voltage ratios of these two converters can reach infinity, but in actuality about three or four, limited by parasitic component effect and controller capability. Consequently, if the voltage ratio of the converter is desired to be over five, then two-stage converter based on the boost converter or the buck-boost converter is utilized, or different converter topologies [1-18] are created.

In [1-10], the Luo converter and its derivatives are presented, whose voltage lift technique is similar to that of the Cuk converter or the SEPIC converter, based on the energy transfer from one inductor via the intermediate capacitor then to the other inductor. Therefore, the transferred energy is mainly determined by the capacitance, thus causing the current stress on the capacitor to be serious. In [11][12], the voltage-boosting converter with very high voltage ratio also uses a capacitor as an energy-transferring medium, similar to the behavior of the Cuk converter or the SEPIC converter, and hence the current stress on the capacitor is also serious. In [13], the voltage-boosting converter, specified with input voltage, output voltage and rated output current being 24V, 200V and 2A, respectively, is presented. Such a converter combines the characteristics of the boost converter and the characteristics of the bootstrap scheme to achieve voltage boosting. The higher the voltage ratio is, the more the number of bootstraps and hence the more the number of diodes and capacitors. However, the surge current occurs as the energy is transferred via large capacitance, and hence the value of the capacitor can not be too large and the corresponding equivalent series resistance (ESR) is relatively large. In [14], the voltage-boosting converter has the voltage ratio of 1/(1-2D) in the continuous conduction mode (CCM), where D is the duty cycle of the main switch. And as compared with the boost converter, this converter is complicated due to four switches required. In [15], the KY converter is presented, but the maximum voltage ratio of such a converter is only two. As for [16-18], the coupled-boost converter is presented, which uses a coupling inductor as an energy-transferring medium. In [18], this converter has the voltage ratio of 1+nD/(1-D). However, in this converter, suppressing the voltage spike created due to the leakage inductance of the coupling inductor is taken into account by

adding an active voltage-clamping circuit which pumps part of the leakage inductance energy to the input. However, for the multi-phase to be considered, the more the number of phases is, the more the number of active voltage-clamping circuits.
Consequently, a new voltage-boosting converter, combining the charge pump and the coupling inductor, is presented herein, together with a passive voltage clamping circuit. There are four main merits in this converter. The first is this converter with high voltage ratio required is simpler in structure than any converter mentioned above. The second is that the primary inductor is magnetized under double the input voltage, thereby causing the input current to be reduced and hence the efficiency to be improved at light load, which is similar to the behavior of the KY converter [19]. The third is that the passive voltage-clamping circuit pumps part of the energy stored in the leakage inductance to the output. The four is that, for the multi-phase to be considered, if the number of phases is N, then only additional N-1 diodes are added. However, there is mainly one demerit in this converter. Since there is one right half-plane zero, the corresponding phase margin is reduced and hence the high-performance control of this converter is not so easy to obtain. In this paper, some mathematical derivations, and simulated and experimental results are offered to demonstrate the effectiveness of the proposed voltage-boosting converter topology.

2. Proposed converter configuration

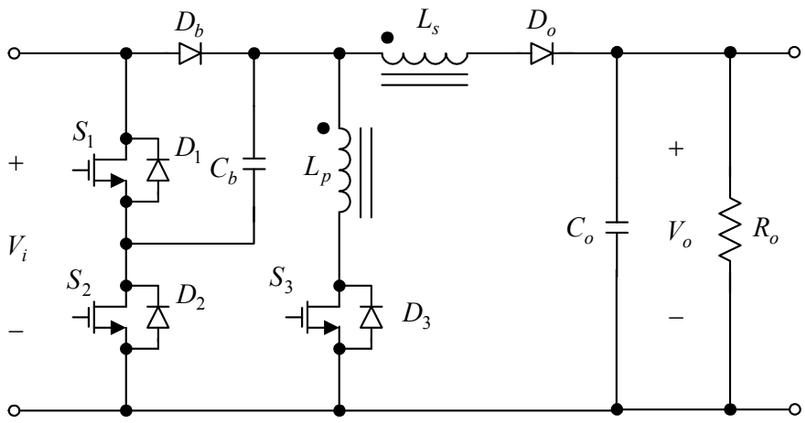

Fig. 1. Proposed voltage-boosting converter without leakage inductance considered.

Fig. 1 shows the proposed voltage-boosting converter. Such a converter contains two cells. One is the charge-pumping cell and the other is the inductance-coupling cell. The former consists of two MOSFET switches S_1 and S_2 with two body diodes D_1 and D_2 connected in parallel respectively, one diode D_b, and one capacitor C_b. The latter is comprised of one main switch S_3 with one body diode D_3 connected in parallel, and one coupling inductor made up of two inductances L_p and L_s, which are coupled together and put at the primary and the secondary, respectively, with the turns ratio n set to N_s/N_p, where N_s is the number of turns in the secondary winding and N_p is the number of turns in the primary winding. The remainder are one output diode D_o, one output capacitor C_o, and one output resistor R_o. However, there is the leakage inductance existing in this coupling inductor, especially for the leakage inductance L_{LK} at the primary, as shown in Fig. 2. Consequently, in Fig. 3, one passive voltage-clamping circuit, containing one inductor L_{sn}, one capacitor C_{sn}, and one diode D_{sn}, is added to this converter, so as to avoid the voltage spike occurring due to L_{LK} and hence destroying the MOSFET switch S_3 eternally. Besides, if the multi-phase concept is

applied to the proposed converter, say, N-phase, then the required passive voltage-clamping circuit is the same as that for the single-phase converter except that the number of additional diodes D_{sn} is N-1.

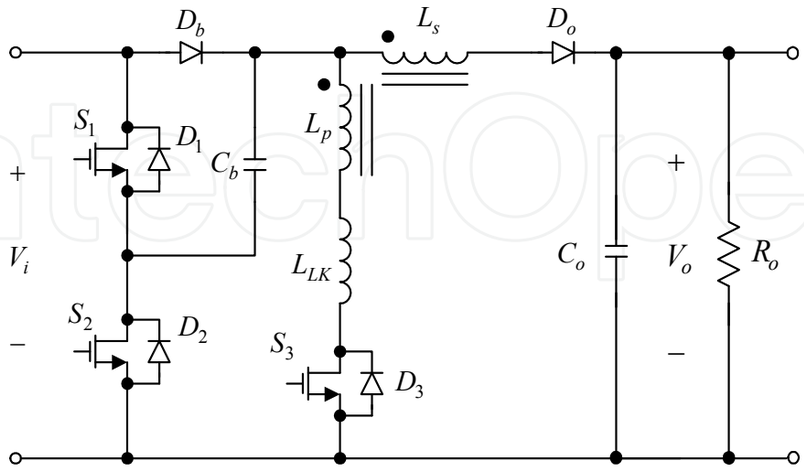

Fig. 2. Proposed voltage-boosting converter with leakage inductance considered.

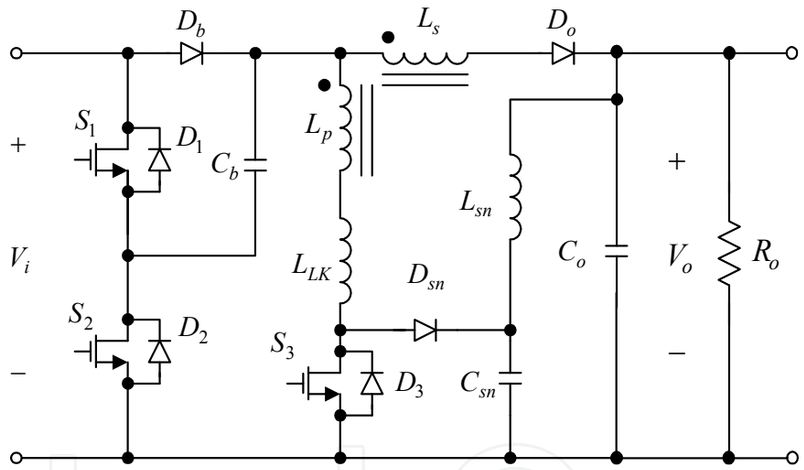

Fig. 3. Proposed voltage-boosting converter with passive voltage-clamping circuit considered.

3. Basic operating principles

Before this section is taken up, it is assumed that the voltage across any MOSFET or diode during the turn-on interval is negligible, there are no blanking times between S_1 and S_2, the voltage across the capacitor C_b is equal to v_i, and the operating mode of this converter is in CCM. As shown in Fig. 4, where T_s is the switching period and the gate driving signals M_1, M_2 and M_3 are used to drive S_1, S_2 and S_3 respectively, the turn-on type of three MOSFET switches is (D, 1-D, D), where D is for S_1 and S_3, 1-D is for S_2, and D is the duty cycle of the pulse-width-modulated (PWM) control signal for S_1. First of all, the basic operating principles for the proposed converter without the passive voltage-clamping circuit are described, and next the basic operating principles of the proposed passive voltage-clamping circuit are illustrated. There are two modes for the former and two modes for the latter.

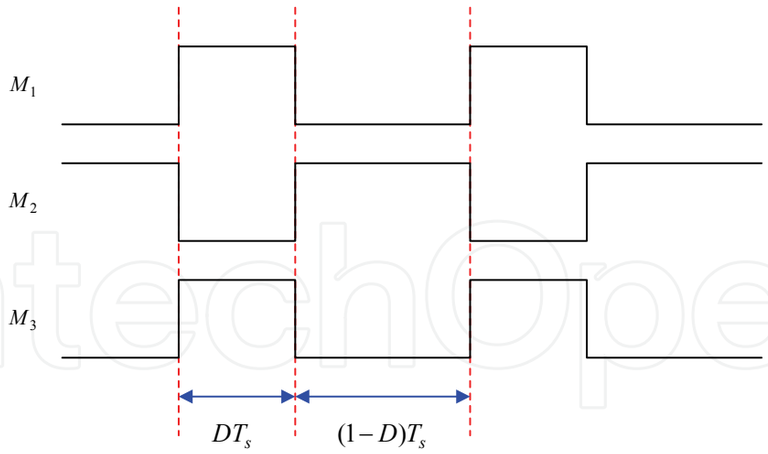

Fig. 4. Ideal timing sequence of gate driving signals M_1, M_2 and M_3 to drive S_1, S_2 and S_3 respectively, without blanking times considered.

A. Basic operating principles of converter

1) *Mode 1:* In Fig. 5, S_1 and S_3 are turned on, but S_2 is turned off. There are two power flows in this mode. One is from the input through S_1 via C_b and then to L_p, S_3 and the ground. The other is from C_o to the ground. Therefore, the voltage across L_p is the input voltage v_i plus the voltage v_i across C_b, thereby causing L_p of the coupling inductor to be magnetized. Besides, C_b is discharged. Also, C_o releases energy into the output. And hence, the corresponding differential equations are:

$$\begin{cases} L_p \dfrac{\partial i_p}{\partial t} = 2v_i \\ C_o \dfrac{\partial v_o}{\partial t} = \dfrac{-v_o}{R_o} \\ i_i = i_p \end{cases} \tag{1}$$

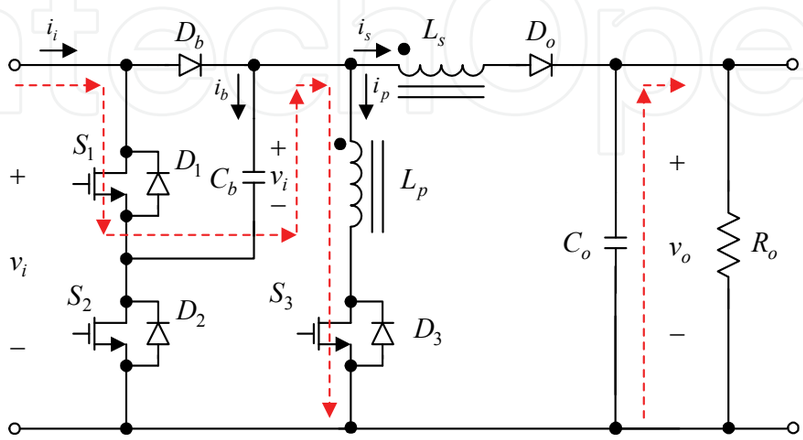

Fig. 5. Power flow of mode 1 without passive voltage-clamping circuit.

2) *Mode 2 :* In Fig. 6, S_1 and S_3 are turned off, but S_2 is turned on. There are two power flows in this mode. One is from the input through C_b via S_2 and then to the ground. The other is from the input through D_b via L_s and then to D_o and the output. Therefore, the voltage across L_s is the input voltage v_i minus the output voltage v_o, thereby causing L_s of the coupling inductor to be demagnetized. Besides, C_b is charged. Also, C_o is energized. And hence, the corresponding differential equations are:

$$\begin{cases} L_s \dfrac{\partial i_s}{\partial t} = v_i - v_o \\ C_o \dfrac{\partial v_o}{\partial t} = i_s - \dfrac{v_o}{R_o} \\ i_i = i_s + i_b \end{cases} \tag{2}$$

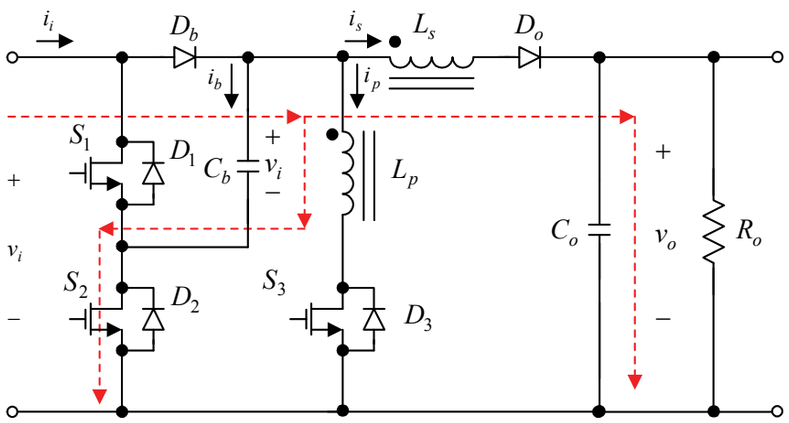

Fig. 6. Power flow of mode 2 without passive voltage-clamping circuit.

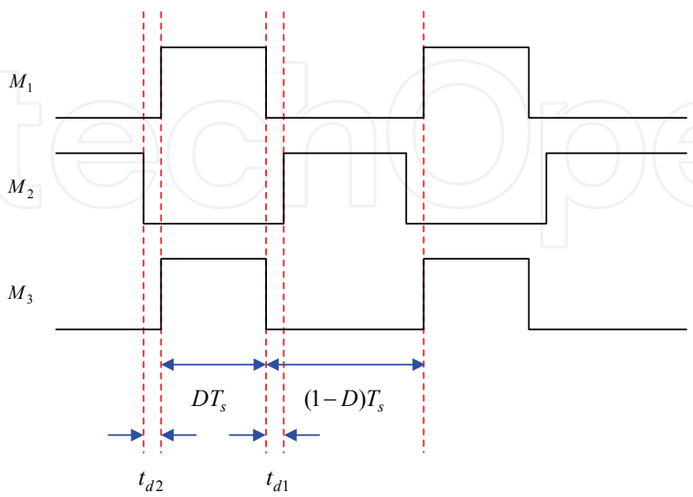

Fig. 7. Ideal timing sequence of gate driving signals M_1, M_2 and M_3 to drive S_1, S_2 and S_3 respectively, with blanking times considered.

However, in practice there are blanking times between S_1 and S_2, as shown in Fig. 7. And hence, there exist additional two modes. One mode, mode 3, locates between mode 1 and mode 2, with the blanking time of t_{d1} considered. The other mode, mode 4, locates after mode 2 before mode 1, with the blanking time t_{d2} considered. These two are to be described as follows.

Applying the voltage-second balance to (1) and (2), the voltage conversion ratio can be obtained to be:

$$\frac{V_o}{V_i} = \frac{(2n-1)D+1}{1-D} \tag{3}$$

3) *Mode 3:* In Fig. 8, S_1, S_2 and S_3 are all turned off, with the delay time of t_{d1} considered. There is only one power flow that is from the ground through C_b via L_s and then to D_o and the output. Therefore, the voltage across L_s is the voltage v_i across C_b minus the output v_o, thereby causing L_s of the coupling inductor to be demagnetized. Besides, C_b is discharged. Also, C_o is energized.

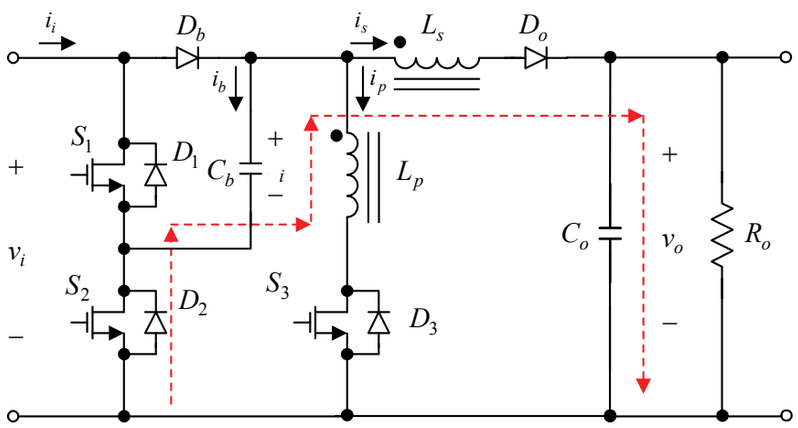

Fig. 8. Power flow of mode 3 without passive voltage-clamping circuit.

4) *Mode 4:* In Fig. 9, S_1, S_2 and S_3 are all turned off, with the delay time of t_{d2} considered. There is only one power flow that is from the input through D_b via L_s and then to D_o and the

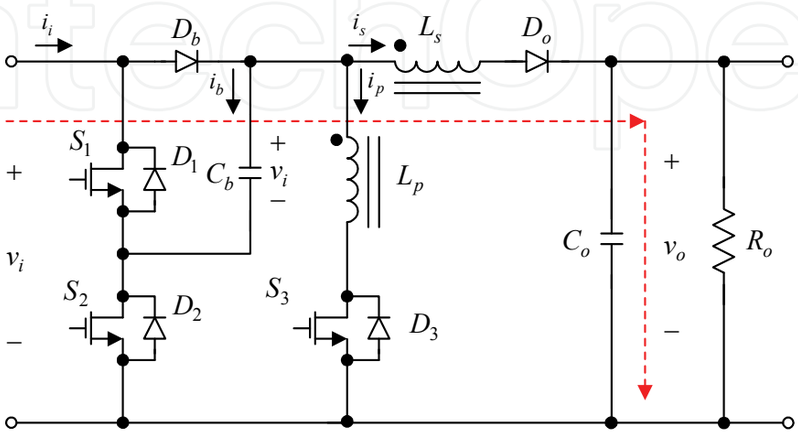

Fig. 9. Power flow of mode 4 without passive voltage-clamping circuit.

output. Therefore, the voltage across L_s is the input voltage v_i minus the output v_o, thereby causing L_s of the coupling inductor to be demagnetized. Besides, C_b lies idle. Also, C_o is charged.

B. Operating principles of passive voltage-clamping circuit

In this subsection, the main description focuses on the behavior of the passive voltage-clamping circuit instead of the behavior of the main power stage.

1) *Mode 1:* In Fig. 10, the moment S_3 is turned off, the energy stored in L_{LK} is released to C_{sn} via D_{sn}.

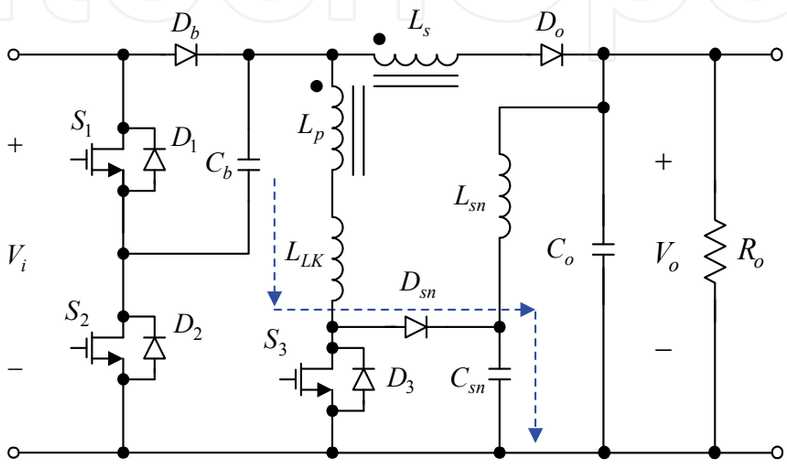

Fig. 10. Power flow of passive voltage-clamping circuit in mode 1.

2) *Mode 2:* In Fig. 11, as soon as S_3 is turned on, the energy stored in C_{sn} is pumped into the output via L_{sn}.

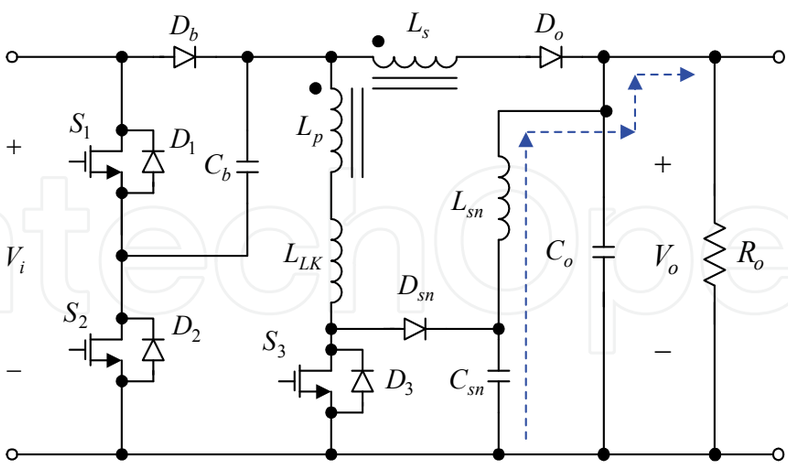

Fig. 11. Power flow of passive voltage-clamping circuit in mode 2.

4. Applied control method

Fig. 12 shows the proposed overall system block diagram for the proposed converter. The one-comparator counter-based PWM control without any analog-to-digital converter (ADC)

based on the field programmable gate array (FPGA) [20][21] is employed herein, and the parameters of the proportional integral (PI) controller, including the proportional gain k_p and the integral gain k_i, are tuned at rated load. In addition, the output voltage information after the voltage divider is obtained through the comparator, and then sent to FPGA having a system clock of 100MHz to create the desired PWM control signals to drive the MOSFET switches after the gate drives.

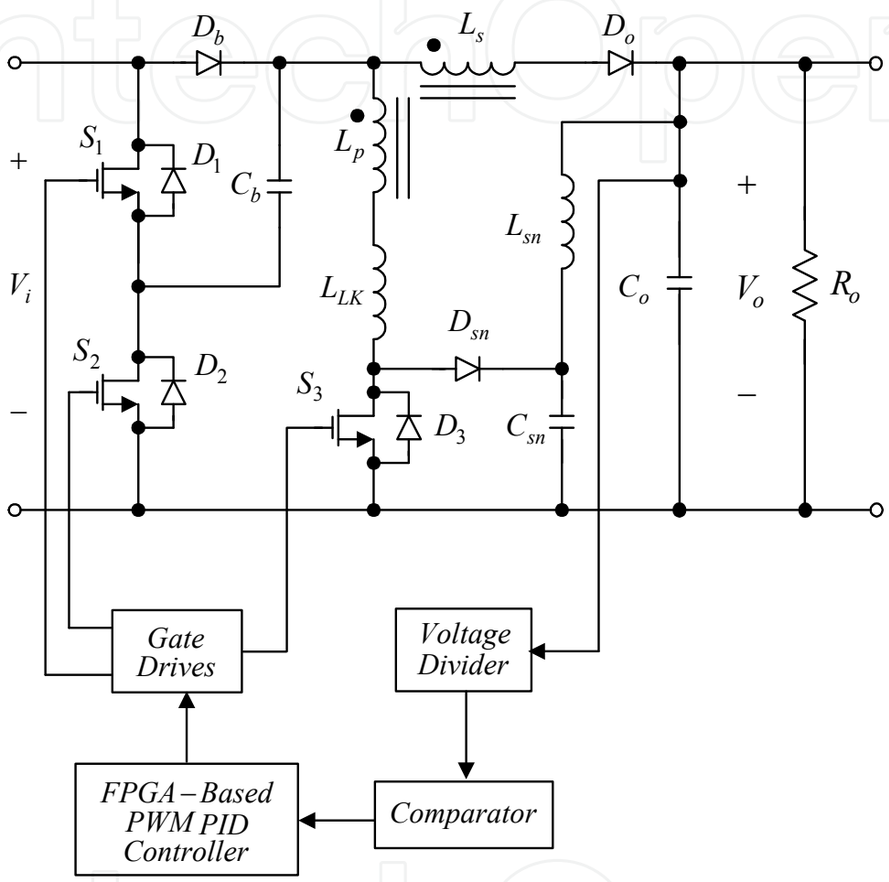

Fig. 12. Overall system block diagram for the proposed converter.

5. Key parameter considerations

Before this section is discussed, there are some specifications to be given as follows: (i) rated DC input voltage V_i is set to 5V; (ii) rated DC output voltage V_o is set to 48V; (iii) rated DC output power $P_{o\text{-}rated}$ is set to 48W; (iv) minimum DC output current $I_{o\text{-}min}$ in the boundary conduction mode (BCM) is 0.15A; (v) switching frequency f_s is chosen to be 195kHz; (vi) turns ratio N_s/N_p of the coupling inductor is set to 5; (vii) one 1000μF electrolytic capacitor is chosen for C_o; (viii) product names of D_b, D_{sn} and D_o are STPS20L25, 3CTQ100 and 3CTQ100, respectively; (ix) product names of S_1, S_2 and S_3 are PHD96NQ03LT, PHD96NQ03LT and IRL3705ZS, respectively; (x) product name of the control IC is EPIC3T100; (xi) PI controller parameters k_p and k_i are set to 0.25 and 0.0625, respectively; and (xii) blanking times t_{d1} and t_{d2} are both set to 100ns.

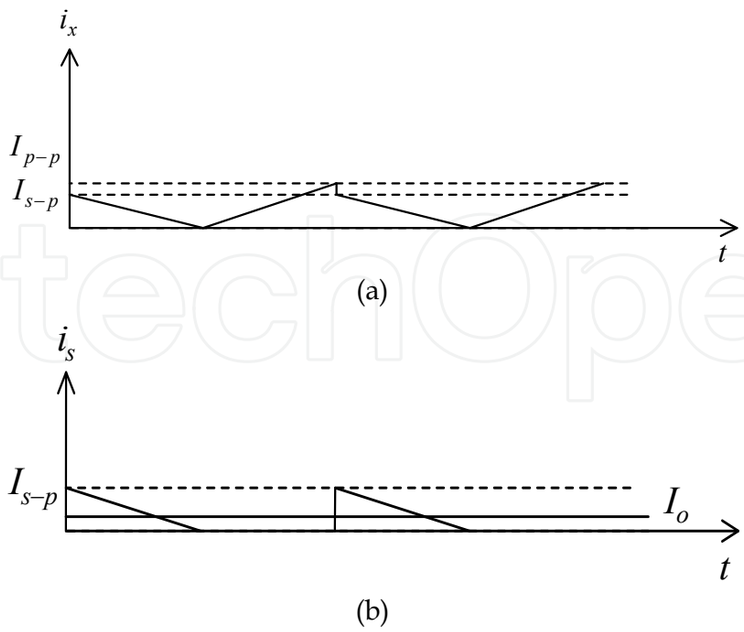

Fig. 13. Current waveforms in BCM: (a) primary-side current plus secondary-side current, i_x; (b) secondary-side current i_s.

A. Design of main power stage

In the main power stage, there are three key parameters to be designed. One is the value of C_b in the charge-pumping cell and the other two are the values of L_p and L_s in the inductance-coupling cell. On condition that this converter works in BCM, corresponding to the minimum load current $I_{o\text{-}min}$, the peak value $I_{p\text{-}p}$ of the current flowing through L_p, shown in Fig. 13, can be expressed to be:

$$I_{p-p} = nI_{s-p} = \frac{2nI_{o-min}}{1-D} \tag{4}$$

where $I_{s\text{-}p}$ is the peak value of the current flowing through L_s.
Consequently, the minimum energy stored in L_p under BCM, $E_{L\text{-}min}$, can be represented as:

$$E_{L-min} = \frac{1}{2}L_p I_{p-p}^2 \geq \frac{1}{2}V_i D T_s I_{p-p} \tag{5}$$

Based on (4) and (5), the value of L_p can be expressed to be:

$$L_p \geq \frac{V_i D(1-D)T_s}{2nI_{o-min}} \tag{6}$$

According to the given specifications and (3) and (6), the value of L_p is calculated to be larger than 4.3μH, and eventually one coupling inductor is chosen with L_p set to 5μH using one T106-18 core with five turns and L_s set to 80μH using the same core with twenty turns.
Besides, there are some assumptions used to obtain the value of C_b as follows: (i) this converter operates at rated load; (ii) C_b is charged to V_i in mode 2; (iii) maximum percentage

of decreased variation in voltage on C_b in discharge, ε, is set to 0.5% in mode 1; (iv) input voltage is an infinite bus, i.e., the input voltage is kept constant and can be represented as infinite capacitance which is much larger than the value of C_b; and (v) converter efficiency η is initially set to 80% at rated load. It is noted that the efficiency is assumed to be 80% at rated load is based on the following reason. Since this coupling inductor behavior is similar to the transformer in the flyback converter and the efficiency of the flyback converter under the traditional control technique is generally about 80%, this is why the efficiency of the proposed converter operating at rated load is roughly chosen to be 80% for the convenience of design of C_b.
Therefore, in mode 1, the energy E_e is extracted from V_i and C_b, and can be expressed as:

$$\begin{aligned} E_e &= \frac{1}{2}C_b\left\{(2V_i)^2 - \left[(2-\varepsilon)V_i\right]^2\right\} \\ &= \frac{1}{2}(4\varepsilon - \varepsilon^2)C_b V_i^2 \end{aligned} \tag{7}$$

Also, in mode 2, the energy E_s is sent to the load, and can be represented as:

$$E_s = \frac{P_{o-rated}(1-D)T_s}{\eta} \tag{8}$$

According to conservation of energy, E_e is not less than E_s, and hence the value of C_b can be expressed to be:

$$C_b \geq \frac{2P_{o-rated}(1-D)T_s}{(4\varepsilon - \varepsilon^2)V_i^2\eta} \tag{9}$$

Based on the given specifications and assumptions and (3) and (9), the value of C_b is calculated to be larger than 362μF, and finally two paralleled 330μF OSCON capacitors connected in parallel with one 22μF MLCC capacitor are selected for C_b to compensate the effect of frequency on the capacitance and the reduction of the equivalent series resistance (ESR).

B. Design of passive voltage-clamping circuit

There are two key parameters to be designed in the passive voltage-clamping circuit. One is the value of C_{sn}, and the other is the value of L_{sn}. Before doing these, we need to measure the value of L_{LK} and set the maximum value of the voltage across C_{sn}, V_{max}, during the turn-off period for S_3 without the voltage spike considered. And hence, based on the following, the minimum value of C_{sn} can be obtained to be:

$$\frac{1}{2}C_{sn}V_{max}^2 \geq \frac{1}{2}L_{LK}I_{p-max}^2 \tag{10}$$

By rearranging (10), the resulting value of C_{sn} can be obtained to be:

$$C_{sn} \geq \frac{L_{LK}I_{p-max}^2}{V_{max}^2} \tag{11}$$

where $I_{p\text{-}max}$ is the maximum value of the current flowing through L_p at rated load.
As for the value of L_{sn}, the relationship between the time required for the voltage across C_{sn} to fall from the maximum value to zero without the voltage spike considered and the turn-off period for S_3 can be expressed as

$$(1-D)T_s \geq 0.5\pi\sqrt{L_{sn}C_{sn}} \tag{12}$$

By rearranging (12), the resulting value of L_{sn} can be found to be

$$L_{sn} \leq \frac{4(1-D)^2 T_s^2}{\pi^2 C_{sn}} \tag{13}$$

Based on (13), the measured value of 1.8μH for L_{LK}, V_{max} set to double the input voltage, and other given and calculated values, the resulting minimum value of C_{sn} is worked out to be 1.98μF and finally the value of C_{sn} is set to 2.2μF whereas the resulting maximum value of L_{sn} is figured out to be 1.42μH and eventually the value of L_{sn} is set to 1μH.

6. Simulated and experimental results

Before some experimental results are provided, a simulated result at startup based on MATLAB/SIMULINK/SIMPOWERSYSTEMS for the proposed converter operating under the open loop are provided to verify its feasibility, and after this, some experimental results under the closed loop are utilized to demonstrate the effectiveness of this converter. Therefore, Fig. 14 shows the simulated output voltage of the proposed converter under open-loop control during startup. It can be seen that the output voltage of this converter can stably rise to the neighborhood of the prescribed value.

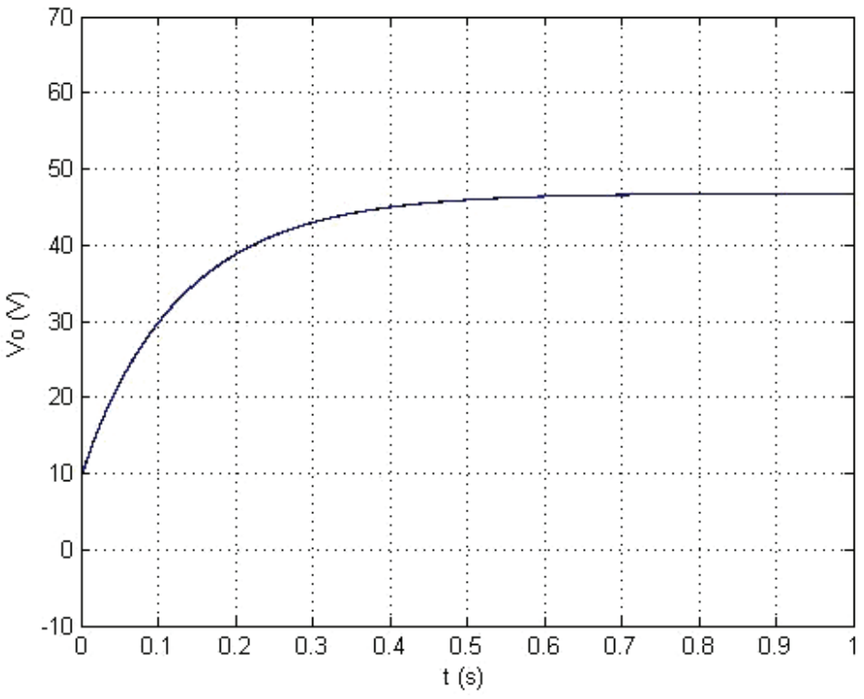

Fig. 14. Simulated output voltage during startup.

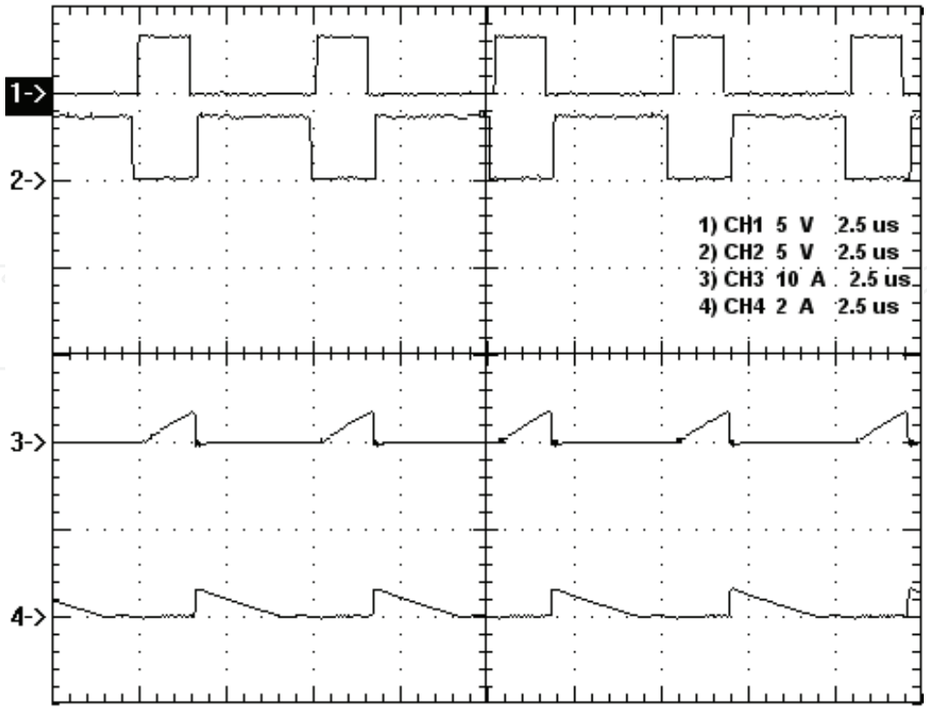

Fig. 15. Under 15% of the rated load: (1) gate driving signal for S_3; (2) gate driving signal for S_2; (3) current in L_p; (4) current in L_s.

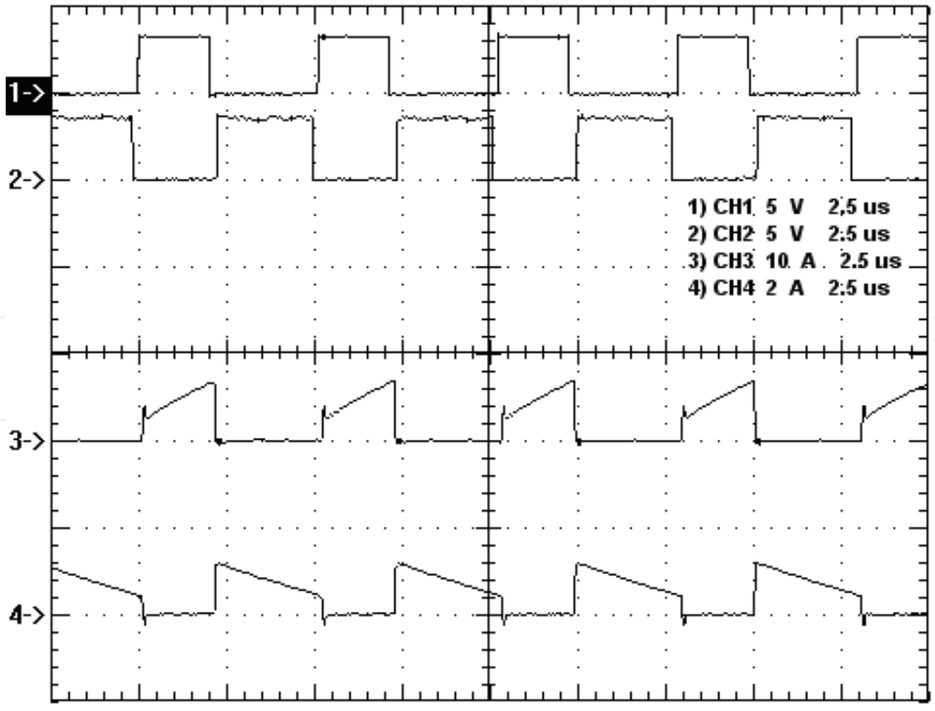

Fig. 16. Under 50% of the rated load: (1) gate driving signal for S_3; (2) gate driving signal for S_2; (3) current in L_p; (4) current in L_s.

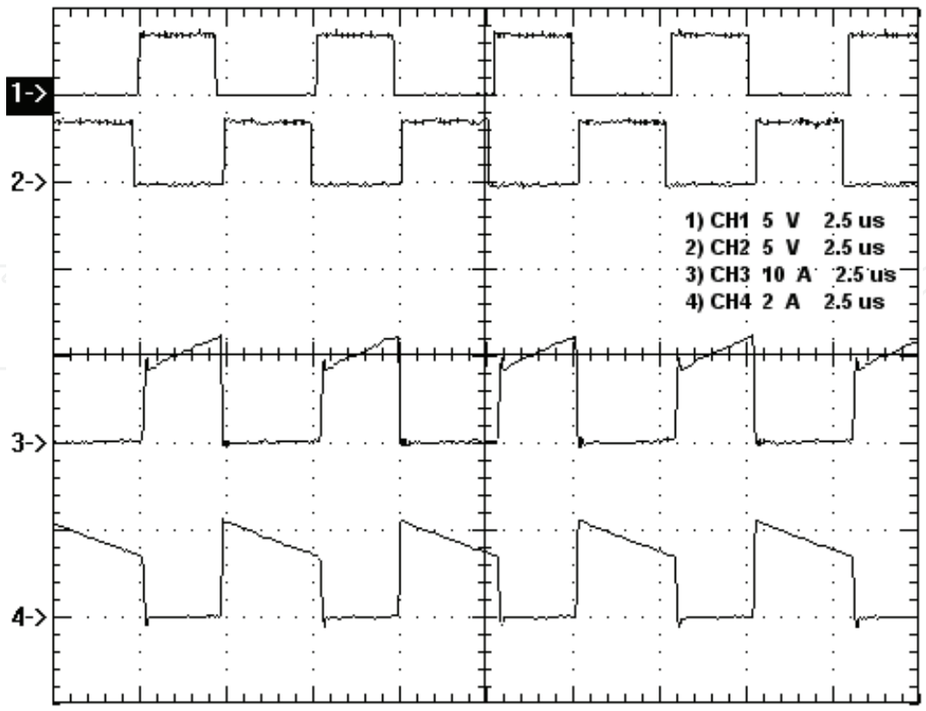

Fig. 17. Under the rated load: (1) gate driving signal for S_3; (2) gate driving signal for S_2; (3) current in L_p; (4) current in L_s.

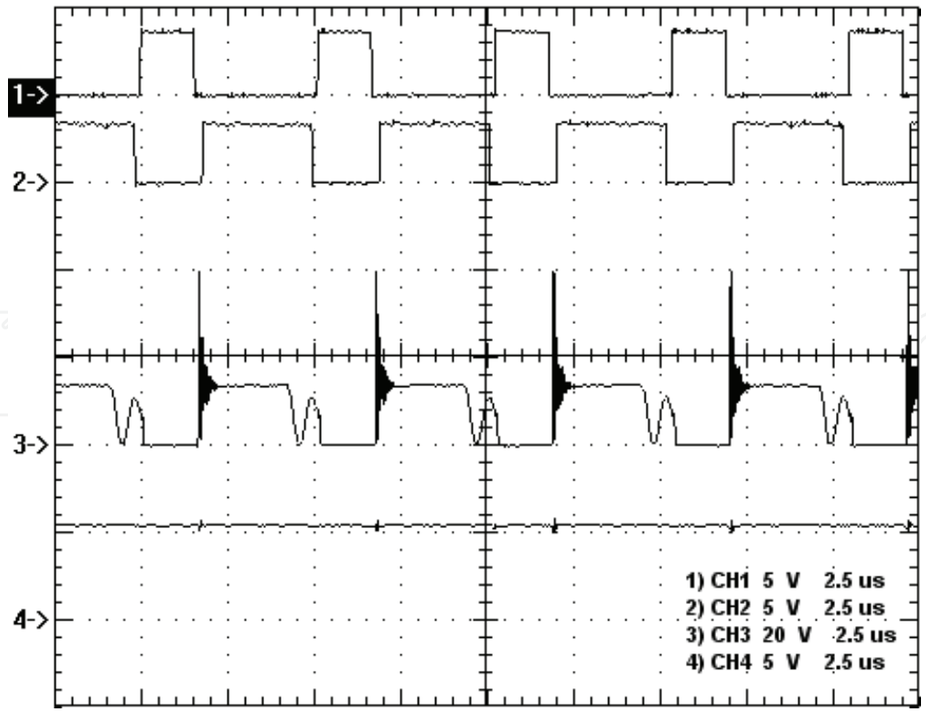

Fig. 18. Under 15% of the rated load: (1) gate driving signal for S_3; (2) gate driving signal for S_2; (3) voltage on S_3; (4) voltage on C_b.

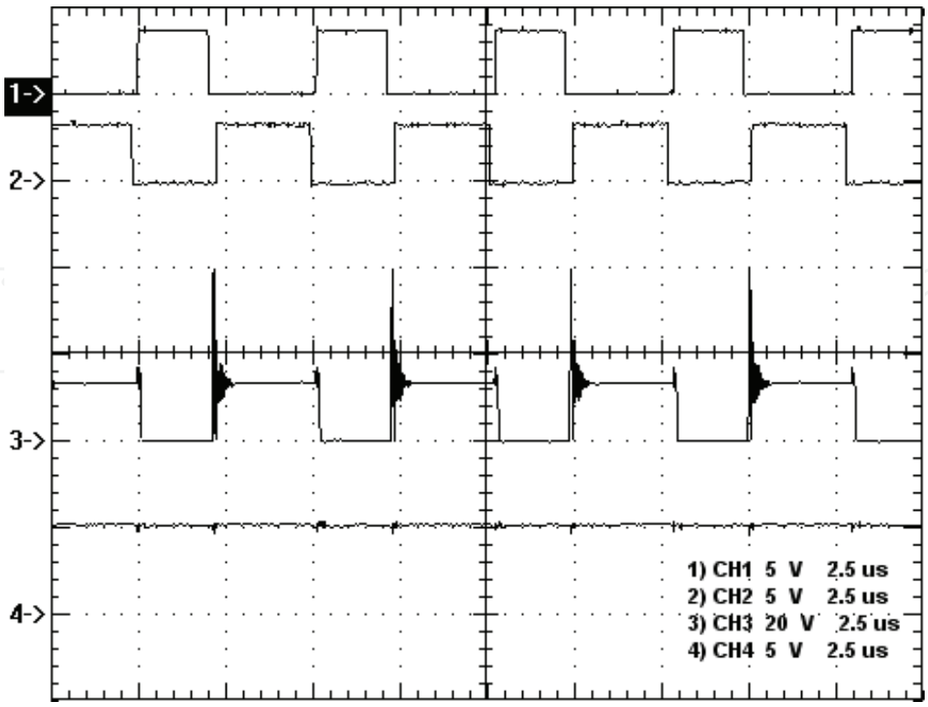

Fig. 19. Under 50% of the rated load: (1) gate driving signal for S_3; (2) gate driving signal for S_2; (3) voltage on S_3; (4) voltage on C_b.

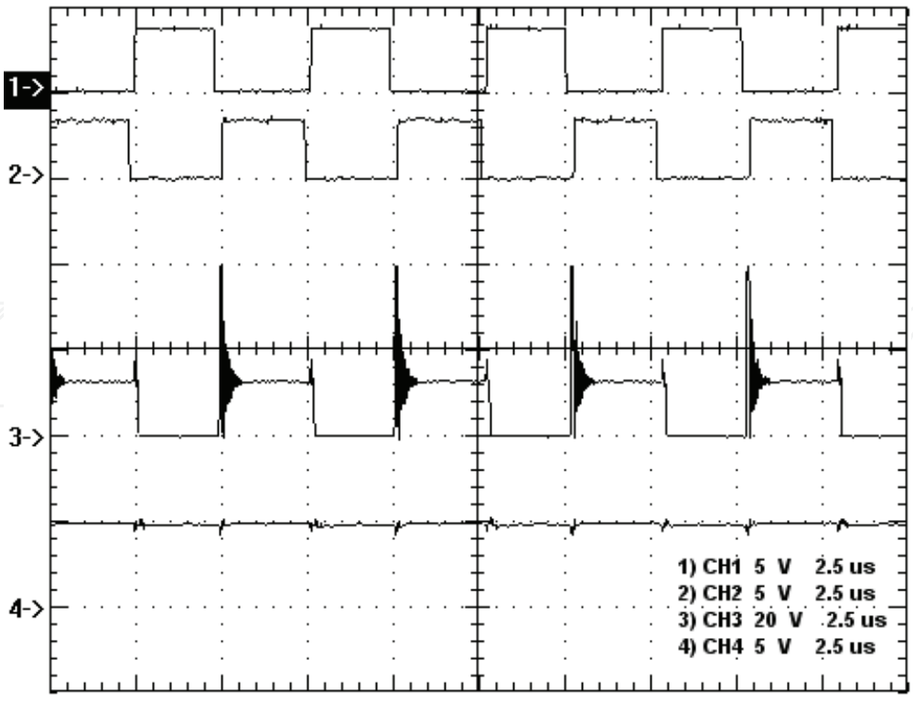

Fig. 20. Under the rated load: (1) gate driving signal for S_3; (2) gate driving signal for S_2; (3) voltage on S_3; (4) voltage on C_b.

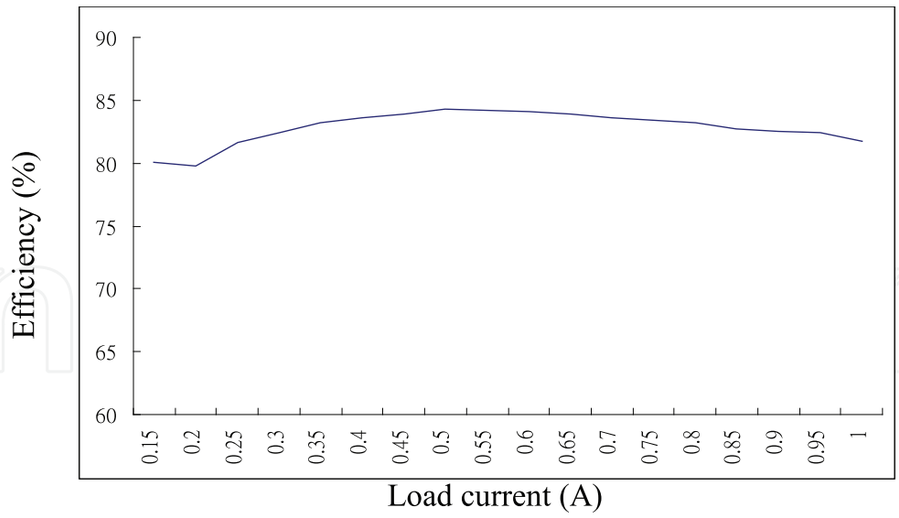

Fig. 21. Efficiency versus load current.

Afterwards, some experimental waveforms shown in Figs. 15 to 21 are provided to verify the performance of the proposed circuit topology. Figs. 15 to 17 depict the PWM gate driving signals for S_3 and S_2 and the currents in L_p and L_s, under 15%, 50% and 100% of the rated load respectively. It is noted that the converter under 15% of rated load operates in DCM, which does not correspond to the design specifications. This is because the inductance is reduced due to the high switching frequency. Figs. 18 to 20 show the gate driving signals for S_3 and S_2, the voltage on S_3 and the voltage on C_b, under 15%, 50% and 100% of the rated load respectively. It is noted that the more the load current, the lower the voltage on S_3. As for the voltage spike on S_3, it is due to the turn-on delay created from the diode D_{sn}. Besides, the voltage across S_3 is larger than double the input voltage prescribed. This is because the value of C_{sn} is reduced due to high frequency or there exists capacitance tolerance in C_{sn}. According to the mention above, it is evident that the proposed voltage-boosting converter can stably operate under closed-loop control.

On the other hand, Fig. 21 displays the curve of efficiency versus load current. It is noted that unlike the traditional voltage-boosting converter, the proposed voltage-boosting possesses an almost flat range of the efficiency from minimum load to rated load. This is because the charge-pumping cell is used. To explain lucidly, the primary inductance of the coupling inductor is magnetized by double the input voltage, thereby causing the input current to be reduced, and this behavior is similar to the KY converter.

7. Conclusion

A new voltage-boosting converter, combining the charge pump and the coupling inductor, is proposed herein, together with a passive voltage-clamping circuit. Conclusions are summarized as follows:

1. This converter with high voltage ratio required is simpler in structure than any other converter mentioned in Sec. I.
2. The primary inductor is magnetized under double the input voltage, thereby causing the input current to be reduced and hence the efficiency to be upgraded at light load, and this behavior is similar to the KY converter.
3. The passive voltage-clamping circuit pumps part of the energy stored in the leakage inductance to the output.

4. For the multi-phase to be considered, if the number of phases is N, then only additional N-1 diodes are added.

8. References

[1] F. L. Luo, Ye Hong and M. H. Rashid, "Four quadrant operating Luo-converters," *IEEE PESC'00*, vol. 2, pp. 1047-1052, 2000.

[2] Fang Lin Luo, "Luo-converters, voltage lift technique," *IEEE PESC'98*, vol. 2, pp. 1783-1789, 1998.

[3]Xiaofan Chen, Fang Lin Luo and Ye Hong, "Modified positive output Luo converters," *IEEE PEDS'99*, vol. 1, pp. 450-455, 1999.

[4] F. L. Luo, H. Ye and M. H. Rashid, "Multiple-quadrant Luo-converters," *IEE Proc. Electr. Power Appl.*, vol. 149, no. 1, pp. 9-18, 2002.

[5] F. L. Luo and H. Ye, "Positive output cascade boost converters," *IEE Proc. Electr. Power Appl.*, vol. 151, no. 5, pp. 590-606, 2004.

[6] F. L. Luo and H. Ye, "Ultra-lift Luo-converter," *IEE Proc. Electr. Power Appl.*, vol. 152, no. 1, pp. 27-32, 2005.

[7] F. L. Luo, "Seven self-lift DC-DC converters, voltage lift technique," *IEE Proc. Electr. Power Appl.*, vol. 148, no. 4, pp. 329-338, 2001.

[8] F. L. Luo and H. Ye, "Negative output super-lift converters," *IEEE Trans. Power Electron.*, vol. 18, no. 5, pp. 1113-1121, 2003.

[9] F. L.Luo and H. Ye, "Positive output super-lift converters" *IEEE Trans. Power Electron.*, vol. 18, no. 1, pp. 105-113, 2003.

[10] F. L. Luo and H. Ye, "Positive output multiple-lift push-pull switched-capacitor Luo-converters" *IEEE Trans. Ind. Electron.*, vol. 51, no. 3, pp. 594-602, 2004.

[11] Wai Rong-Jong and Duan Rou-Yong, "High step-up converter with coupled-inductor," *IEEE Trans. Power Electron.*, vol. 20, no. 5, pp. 1025-1035, 2005.

[12] Wai Rong-Jong and Duan Rou-Yong, "High step-up coupled-inductor-based converter using bi-direction energy transmission," IEEE PESC'05, pp. 406-412, 2005.

[13] R.Gules, L. L. Pfitscher and L. C. Franco, "An interleaved boost DC-DC converter with large conversion ratio," *IEEE ISIE '03*, vol. 1, pp. 411-416, 2003.

[14] G. Yao, A. Chen and X. He, "Soft switching circuit for interleaved boost converters," *IEEE Trans. Power Electron.*, vol. 22, no. 1, pp. 80-86, Jan. 2007.

[15] K. I. Hwu and Y. T. Yau, "A novel voltage-boosting converter: KY converter," *IEEE APEC'07*, vol. 1, pp. 368-372, 2007.

[16] Rong-Jong Wai, Chung-You Lin, Rou-Yong Duan and Yung-Ruei Chang, "High-efficiency DC-DC converter with high voltage gain and reduced switch stress," IEEE Trans. Ind. Electron., vol. 54, pp. 354-364, Feb. 2007.

[17] Tsai-Fu Wu, Yu-Sheng Lai, Jin-Chyuan Hung and Yaow-Ming Chen, "Boost converter with coupled inductors and buck-boost type of active clamp," IEEE Trans. Ind. Electron., vol. 55, pp. 154-162, Jan. 2008.

[18] Qingbo Hu and Zhengyu Lu, "A novel step-up VRM—Two-phase interleaved coupled-boost converter," IEEE PESC'06, pp. 1-5, 2006.

[19] K. I. Hwu and Y. T. Yau, "KY converter and its derivatives," IEEE Trans. Power Electron., vol. 24, no. 1, pp. 128-137, 2009.

[20] K. I. Hwu and Y. T. Yau, "Applying a counter-based PWM control scheme to an FPGA-based SR forward converter," *IEEE APEC'06*, vol. 3, pp. 1396-1400, 2006.

[21] K. I. Hwu and Y. T. Yau, "Improvement of one-comparator counter-based PWM control by applying a sawtoothed wave injection method," *IEEE APEC'07*, vol. 1, pp. 478-481, 2007.

Paths to Sustainable Energy
Edited by Dr Artie Ng

ISBN 978-953-307-401-6
Hard cover, 664 pages
Publisher InTech
Published online 30, November, 2010
Published in print edition November, 2010

The world's reliance on existing sources of energy and their associated detrimental impacts on the environment- whether related to poor air or water quality or scarcity, impacts on sensitive ecosystems and forests and land use - have been well documented and articulated over the last three decades. What is needed by the world is a set of credible energy solutions that would lead us to a balance between economic growth and a sustainable environment. This book provides an open platform to establish and share knowledge developed by scholars, scientists and engineers from all over the world about various viable paths to a future of sustainable energy. It has collected a number of intellectually stimulating articles that address issues ranging from public policy formulation to technological innovations for enhancing the development of sustainable energy systems. It will appeal to stakeholders seeking guidance to pursue the paths to sustainable energy.

InTech Europe
University Campus STeP Ri
Slavka Krautzeka 83/A
51000 Rijeka, Croatia
Phone: +385 (51) 770 447
Fax: +385 (51) 686 166
www.intechopen.com

InTech China
Unit 405, Office Block, Hotel Equatorial Shanghai
No.65, Yan An Road (West), Shanghai, 200040, China
中国上海市延安西路65号上海国际贵都大饭店办公楼405单元
Phone: +86-21-62489820
Fax: +86-21-62489821

IntechOpen